nature materials

ARTICLES

https://doi.org/10.1038/s41563-021-01124-x

Highly compressible glass-like supramolecular polymer networks

Zehuan Huang, Xiaoyi Chen, Stephen J. K. O'Neill, Guanglu Wu, Daniel J. Whitaker, Jiaxuan Li, Jade A. McCune and Oren A. Scherman ✉

Supramolecular polymer networks are non-covalently crosslinked soft materials that exhibit unique mechanical features such as self-healing, high toughness and stretchability. Previous studies have focused on optimizing such properties using fast-dissociative crosslinks (that is, for an aqueous system, dissociation rate constant $k_d > 10\,s^{-1}$). Herein, we describe non-covalent crosslinkers with slow, tuneable dissociation kinetics ($k_d < 1\,s^{-1}$) that enable high compressibility to supramolecular polymer networks. The resultant glass-like supramolecular networks have compressive strengths up to 100 MPa with no fracture, even when compressed at 93% strain over 12 cycles of compression and relaxation. Notably, these networks show a fast, room-temperature self-recovery (< 120 s), which may be useful for the design of high-performance soft materials. Retarding the dissociation kinetics of non-covalent crosslinks through structural control enables access of such glass-like supramolecular materials, holding substantial promise in applications including soft robotics, tissue engineering and wearable bioelectronics.

Supramolecular polymer networks (SPNs) are a class of soft materials composed of linear polymers transiently crosslinked through non-covalent interactions[1,2]. On account of the dynamic nature of these crosslinks, they can serve as sacrificial bonds to dissipate applied energy, thus imparting SPNs with remarkable material properties including high toughness[3], enhanced damping capacity,[4] extreme stretchability[5–7], rapid self-healing[8–10] and reversible mouldability.[11] These superior material properties have led to the use of SPNs as repairable electrodes[12,13], artificial skins[14,15] and drug-delivery devices[16,17]. Although promising strides have been made, the material requirements for some demanding applications have not yet been met. A major limitation of SPNs is achieving extreme compressibility with ultra-high compressive strength and complete self-recovery on short time scales.

Comparing covalently to non-covalently crosslinked polymers, the dissociation kinetics for dynamic networks plays a critical role in the material design and mechanical properties of the SPNs.[1] Craig and coworkers revealed that it is in fact crosslink dynamics, rather than equilibrium thermodynamics, that are paramount in determining the material properties (for example, viscoelasticity) of SPNs[18,19]. They reported that slower dissociation kinetics resulted in more intact crosslinks within a transient network under an applied force, leading to a higher complex modulus. Holten-Anderson et al. further demonstrated control over hierarchical polymer mechanics through tuning the relative ratio of two kinetically distinct metal-ligand crosslinks, which allowed for decoupling of the material mechanics from crosslink structure[20]. These pioneering reports established the basis for understanding the relationship between crosslink kinetics and SPN material properties.

Most reported systems focus on the fabrication of rubber-like SPNs, exploiting the relatively fast dissociation kinetics (that is, for an aqueous system, dissociation rate constant $k_d > 10\,s^{-1}$) of non-covalent crosslinks to achieve desirable material properties such as stretchability and self-healing. The short lifetime ($\tau = k_d^{-1}$) of the crosslinks within these materials limits their dynamic mechanical properties in both the viscous flow and rubber-like regions as the equilibrium is shifted towards the dissociated state (Fig. 1a left, grey). We postulated that extending the lifetime of the crosslinks within a transient network ($k_d < 1\,s^{-1}$) would allow us to access SPNs that acted as a glass-like material at room temperature (Fig. 1a right, blue). Accessing such materials, where the equilibrium is shifted towards an associated state, would improve resistance to applied forces, thus endowing the material with enhanced compressive strength, a current limitation of SPNs.

In the last decade, various non-covalent interactions have been used as dynamic crosslinks for the construction of SPNs within viscous flow and rubber-like ranges. Among them, dynamic networks held together through host–guest interactions have shown particular promise and attracted significant interest on account of their facile and modular design.[21,22] A variety of macrocyclic hosts including crown ethers[23,24], cyclodextrins[25,26], pillar[n]arenes[27–29] and cucurbit[n]urils (CB[n]s)[30,31] have been exploited as crosslinkers for the construction of SPNs. Owing to the high binding affinities and wide scope of guest moieties, CB[n]-mediated host–guest interactions have been used extensively in the design and fabrication of functional supramolecular systems[32–37]. Recently, we reported a CB[8]-enhanced phenyl-perfluorophenyl polar–π interaction, and successfully demonstrated its use as a non-covalent crosslink for fabricating robust and transparent SPNs with tuneable viscoelasticity and high stretchability.[38]

Here, we aim to advance this interaction to devise a series of non-covalent crosslinkers with slow dissociation kinetics, distinct from previous reports. Controlling k_d to be $<1\,s^{-1}$ would expand the dynamic mechanics of the resultant materials towards the glass-like range (Fig. 1a), addressing the poor compressibility of SPNs. To this end, we based our crosslink design on CB[8]-mediated ternary complexation, whereby modification of the second guest determines the k_d of the dynamic crosslink (Fig. 1b,c). We envisioned that the dissociative kinetics of the dynamic crosslinks (host–guest complexes) could be tuned by changing the hydrophobic structure of the phenyl group of the second guest (RBVI). To slow k_d, a stronger enthalpic driving force is needed for the second guest

Melville Laboratory for Polymer Synthesis, Yusuf Hamied Department of Chemistry, University of Cambridge, Cambridge, UK. ✉e-mail: oas23@cam.ac.uk

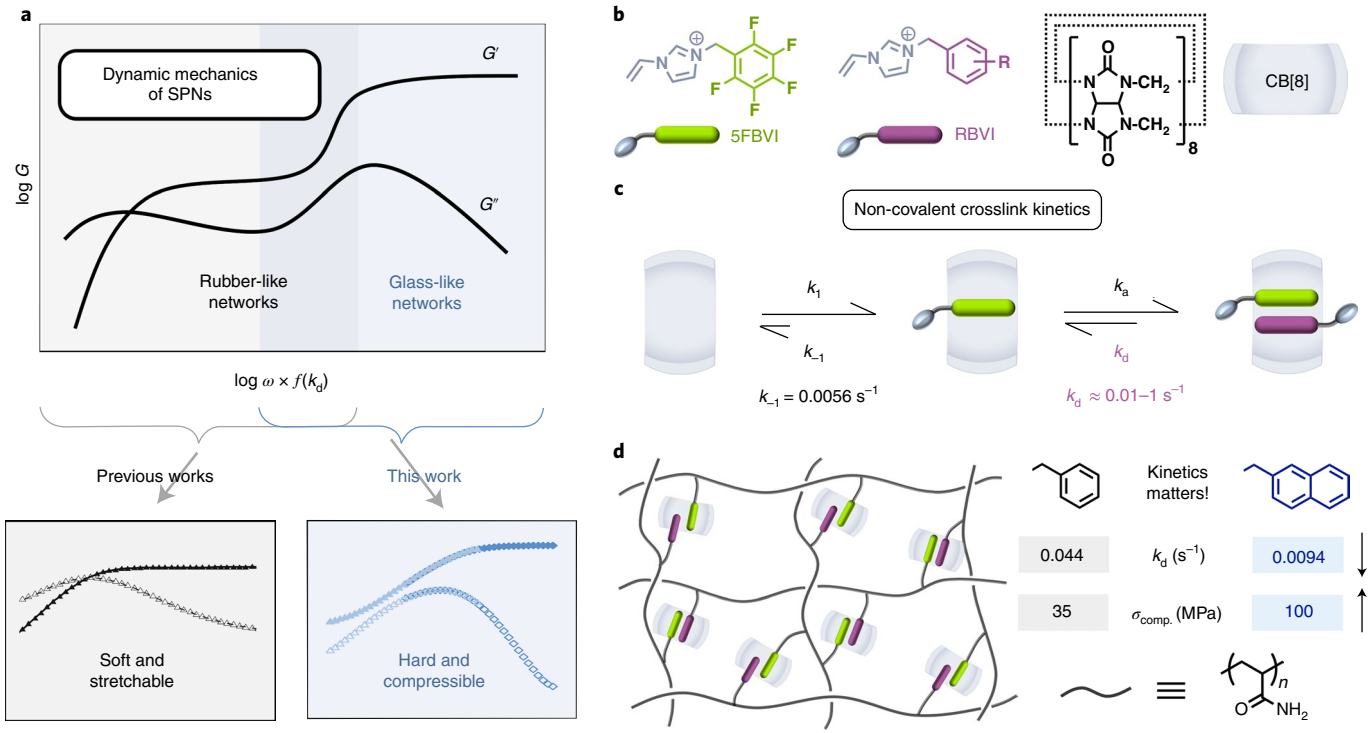

Fig. 1 | Design of glass-like SPNs. a, Schematic overview of the frequency (ω)-dependent dynamic mechanics of SPNs (top) including two real data sets of a reported SPN (left, grey)[20] and this report (right, blue). **b**, Molecular structures of perfluorophenyl (5FBVI), substituted phenyl (RBVI) guests and the host macrocycle (cucurbit[8]uril, CB[8]). **c**, Ternary complexation equilibrium of host-enhanced polar–π interactions including first and second association and their related kinetic parameters (k_1, first-step association constant; k_{-1}, first-step dissociation constant). **d**, Supramolecular polyacrylamide networks crosslinked by the above interactions and two RBVI guests that exhibit slow-dissociative kinetics and high compressive strengths ($\sigma_{comp.}$).

association (k_a) to release more of the conformationally restricted water from the CB[8] cavity.[39] Increasing hydrophobic volume of the second guest can achieve this, which leads to substantial retardation of dissociative process, in accordance with the Bell–Evans–Polanyi principle[40,41].

Quantification of crosslink dissociation kinetics

A library of second guests functionalized with either different substituents on the phenyl group or expanded aromatic moieties were designed and synthesized (Fig. 2a). Binding of each guest to CB[8] was investigated through isothermal titration calorimetry (ITC) to quantify the thermodynamics and kinetics of the second association event (Supplementary Table 1). Titration of each guest into a solution of precomplexed 5FBVI-CB[8] resulted in a clear transition at a molar ratio of 1.0 in all cases (Fig. 2b and Supplementary Figs. 15 and 16). In comparison to parent benzyl vinylimidazolium (BVI, red), introduction of either a hydrophobic chlorine atom (4-chlorobenzyl vinylimidazolium, ClBVI, black) or extension of fused aromatic ring (2-napthylmethyl vinylimidazolium, NVI, blue) resulted in release of more conformationally restricted water from the CB[8] cavity, increasing the binding affinity and retarding the dissociative kinetics. The kinITC method[42] was used to analyse the equilibration time of each titration at different molar ratios (Fig. 2c and Supplementary Fig. 17). The dissociation rate constants (k_d) were obtained through fitting these plots to determine the crosslink dissociation kinetics.

To understand the structure–property relationship, the association constant log K_{eq} of the crosslink as well as its dissociation rate constant log k_d were plotted against the octanol/water partition coefficient (log P) of their corresponding toluene derivatives[43], a common parameter used to evaluate hydrophobicity (Fig. 2d,e, respectively). As shown in Fig. 2d, log P displayed a positive correlation with log K_{eq} and a negative correlation with log k_d (Fig. 2e). This indicated that increasing the hydrophobicity of second guests can substantially enhance the association affinity and simultaneously retard the dissociation kinetics for the ternary complex. In contrast to the unsubstituted BVI, NVI was found to be the most hydrophobic second guest and exhibited the highest K_{eq} and lowest k_d values. The data obtained show that K_{eq} and k_d of these non-covalent crosslinks can be tuned over a wide range from 10^3 to $10^6\,M^{-1}$ and 0.01 to $1\,s^{-1}$, respectively. This confirms that exploiting CB[8]-enhanced phenyl-perfluorophenyl polar–π interactions with a library of derivatized second guests results in ternary complexes with extremely slow-dissociative dynamics tuneable over several orders of magnitude through simple molecular design.

To further explore the relationship between thermodynamics and kinetics within host–guest complexes, we compiled previous literature reports that used either cyclodextrins (CD, α or β) or CB[8] within binary or ternary host–guest complexes, Supplementary Table 2, and plotted their log K_{eq} versus log k_d (Fig. 2f). Notably, K_{eq} values of CB[8] host–guest complexes (yellow squares and green circles) were higher than those found for CD (grey diamonds and purple hexagons). The k_d values for CB[8] ternary complexes measured in this work (green circles) were found to be two orders of magnitude lower than any previously reported CD complexes. This confirms that dynamic CB[8] complexes formed through phenyl-perfluorophenyl polar–π interactions with a derivatized hydrophobic second guest result in ultra-high kinetic stability.

Glass-like rheological behaviour

On account of their low k_d values, these crosslinking motifs were used to prepare SPNs (total monomer concentration $C_M = 2.0\,M$; solid content, 21 wt%) in aqueous media. SPNs were prepared through photopolymerization (6 h at 350 nm) of the crosslinker (5FBVI-CB[8]-RBVI,

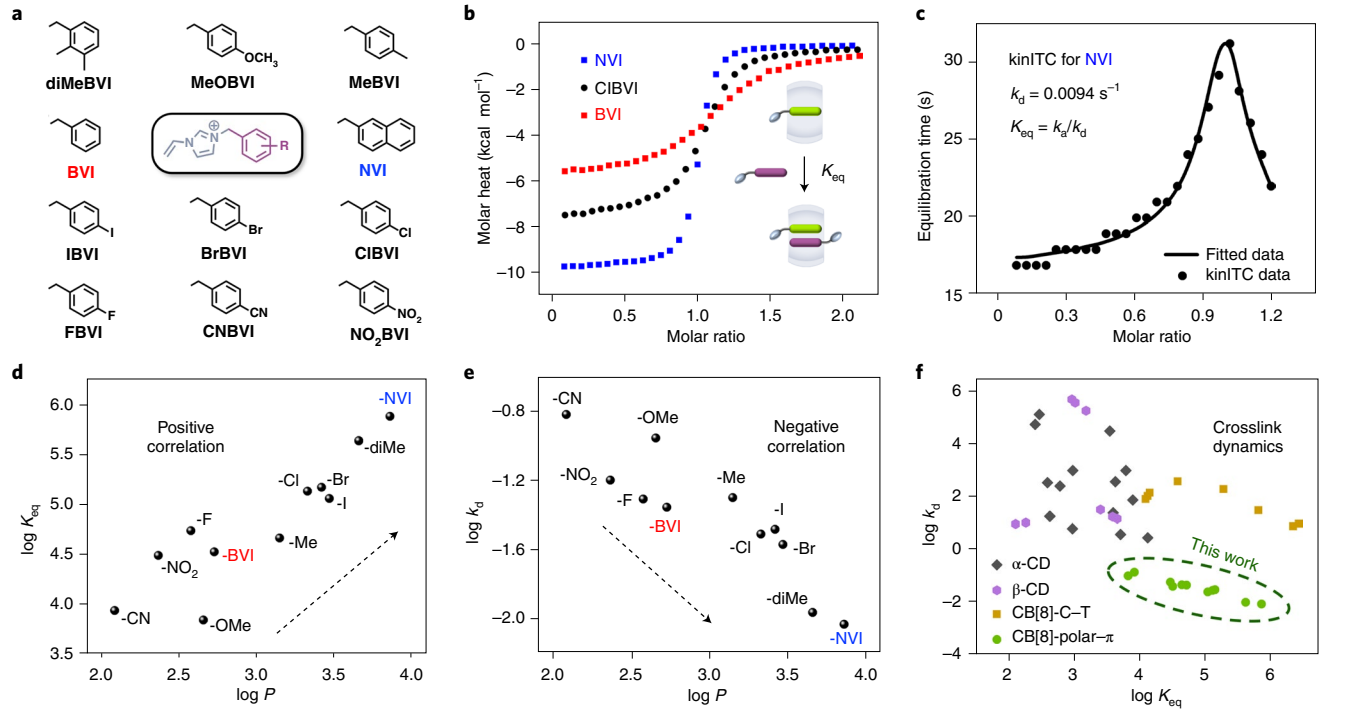

Fig. 2 | Thermodynamic and kinetic properties of slow-dissociative non-covalent crosslinks. a, Molecular structures for all RBVI second guests. **b**, Three typical ITC plots obtained by titration of NVI, ClBVI and BVI (5 mM) into 5FBVI-CB[8] (0.5 mM), respectively. **c**, Representative kinITC plot and fitted curve for incorporation of NVI into 5FBVI-CB[8]. **d**, plot of log K_{eq} for all second guests and log P for their corresponding toluene derivatives. **e**, Plot of log k_d for all second guests and log P for their corresponding toluene derivatives. **f**, Comparison plot of log K_{eq} and log k_d for binary complexes of α-cyclodextrin (α-CD) and β-cyclodextrin (β-CD) as well as ternary complexes of CB[8]-mediated charge-transfer interactions (CB[8]-C–T) and polar-π interactions (CB[8]-polar-π) reported in this work.

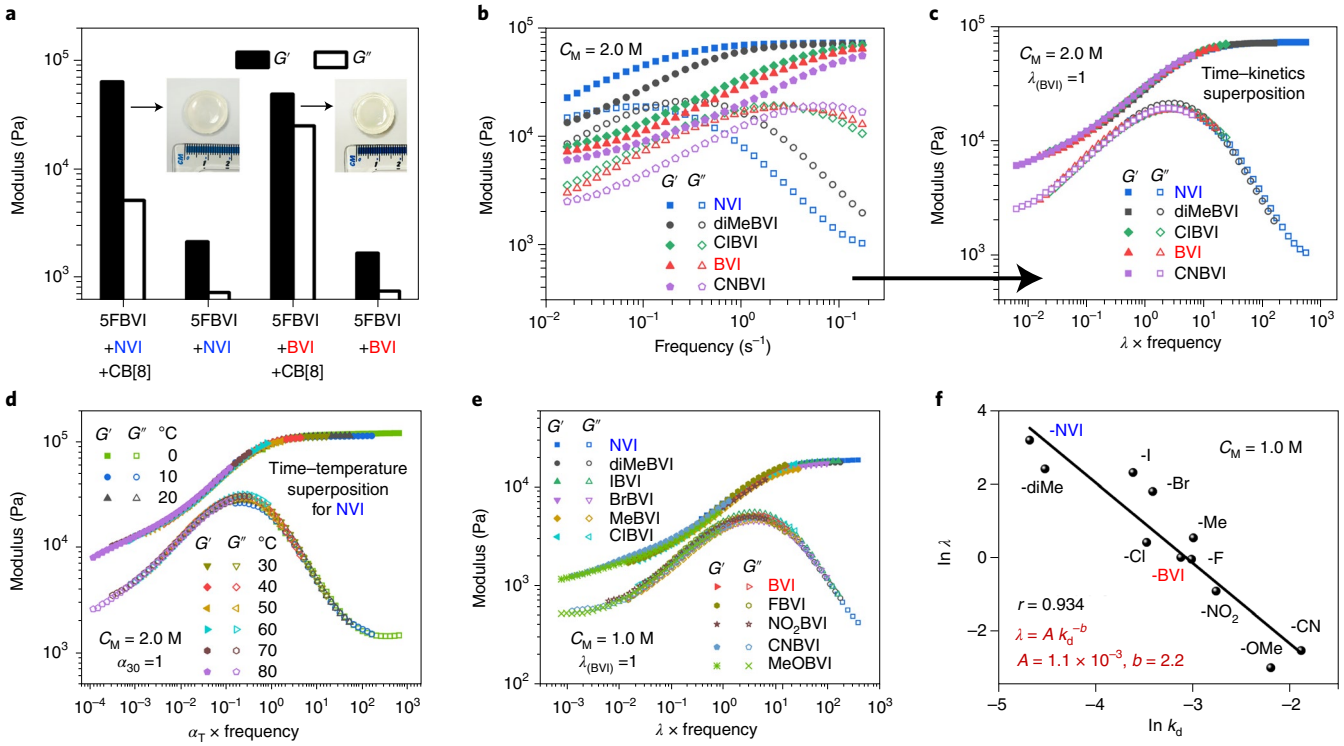

Fig. 3 | Rheological characterization of glass-like SPNs. a, Histogram plot of G' and G'' values for four exemplar SPNs using NVI or BVI crosslinks in the absence and presence of CB[8]. **b**, Frequency-sweep plot of G' and G'' for five SPNs using NVI, diMeBVI, ClBVI, BVI and CNBVI crosslinks, respectively. **c**, Time–kinetics superposition for the frequency sweep shown in **b** scaled by λ. **d**, TTS for NVI-containing SPNs. **e**, Comprehensive frequency-sweep plots of G' and G'' for SPNs crosslinked with 5FBVI-CB[8] and 11 different second guests. **f**, Plots and linear fit for ln λ and ln k_d for all second guests.

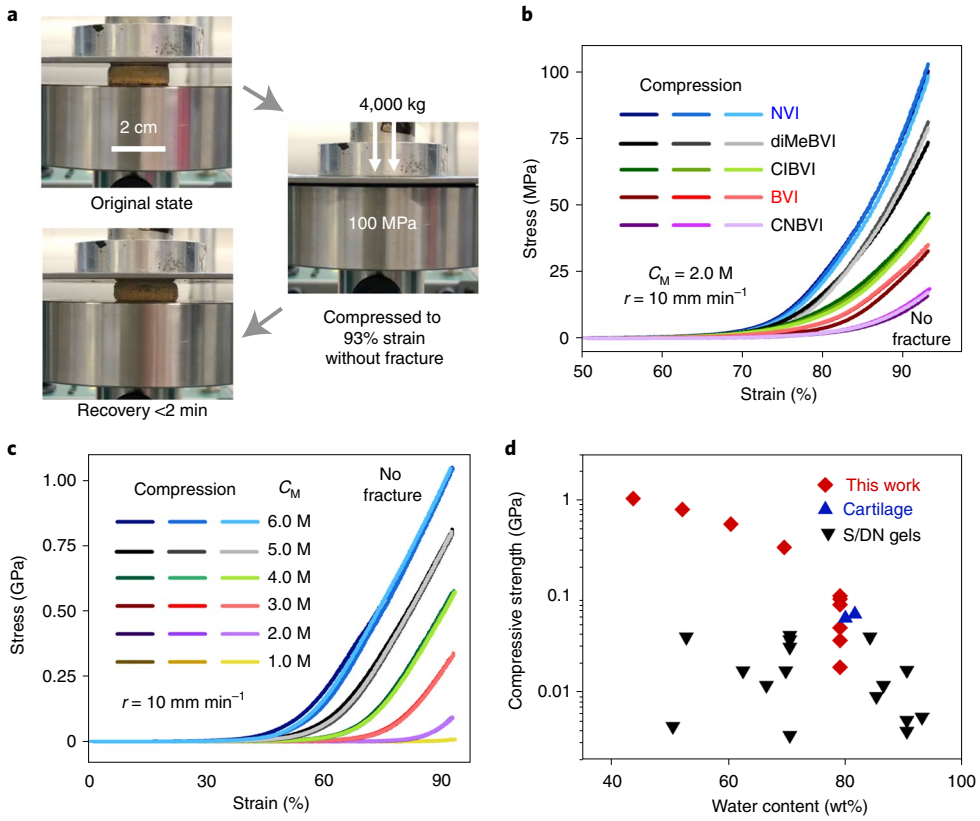

Fig. 4 | Evaluation of compressive properties of glass-like SPNs. a, Photographs of a typical compressive test including uniaxial compression and self-recovery of a cylindrical specimen (22 mm $D \times 7$ mm H). **b**, Compressive stress–strain curves for four SPNs based on 5FBVI-CB[8] and NVI (blue), diMeBVI (black), ClBVI (green), BVI (red) or CNBVI (purple) crosslinks. **c**, Compressive stress–strain curves for six SPNs based on 5FBVI-NVI-CB[8] with different C_M. **d**, Comparison plot of compressive strength and water content for bovine cartilage (blue) and single or double-network gels (black) from previous reports as well as SPNs (red) reported here.

2.5 mol%) in the presence of acrylamide (95 mol%) and characterized by oscillatory rheology to test their dynamic viscoelasticity. As shown in Fig. 3a, SPNs with NVI or BVI crosslinkers in the presence of CB[8] showed higher viscoelasticity with both storage (G') and loss (G'') moduli one to two orders of magnitude above the control networks without CB[8]. G'' of the NVI-crosslinked network was found to be half an order of magnitude lower than that of the BVI network, while both networks displayed a similar G' value (Fig. 3a). This indicates that NVI crosslinks form a more elastic network with lower loss tangent (tan δ) stemming from the slower dissociation of the second binding of NVI compared to BVI.

To interrogate the dynamic viscoelasticity of SPNs held together by crosslinkers with a range of k_d values, frequency-sweep experiments of SPNs constructed with five representative crosslinkers (NVI, 2,3-dimethylbenzyl imidazolium (diMeBVI), ClBVI, BVI and 4-cyanobenzyl imidazolium (CNBVI)) were carried out (Fig. 3b). To decouple the dynamic viscoelasticity from any structural differences of the crosslinkers in the data shown in Fig. 3b, time–kinetics superposition analysis was used through the introduction of a scaling factor (λ) with BVI as the reference (Fig. 3c). This showed a frequency-sweep plot displaying an extended and continuous transition of both G' and G'' moduli from the rubber-like into the glass-like range. Accessible through slow-dissociative non-covalent crosslinkers (for example, 5FBVI-CB[8]-NVI), this represents a great advance in the area of supramolecular polymeric materials.

To gain further insight into this observation, we performed time–temperature superposition (TTS) experiments using a SPN formed with 5FBVI-CB[8]-NVI crosslinks. As shown in Fig. 3d, alongside a decrease in temperature from 80 to 0 °C, the NVI-crosslinked network exhibited a continuous transition from a rubber-like to glass-like state, the same trend observed with the time–kinetics superposition plot shown in Fig. 3c. These results indicate that crosslinkers with a higher k_d (that is, diMeBVI, ClBVI, BVI and CNBVI) display analogous behaviour at 20 °C to crosslinkers with a lower k_d (that is, NVI) at higher temperatures (40–80 °C). This demonstration represents a generic approach to engineer the dynamic viscoelasticity of SPNs at room temperature through controlling the crosslinker structure rather than using elevated temperatures.

To further quantify the relationship between λ and k_d, we carried out frequency-sweep experiments using the full range of 5FBVI-CB[8]-RBVI crosslinkers (Fig. 2a). Using BVI as a reference second guest, time–kinetics superposition analysis was used (Fig. 3e), which showed a clear trend from rubber-like to glass-like states, similar to that observed in Fig. 3c. These data further validate our control over the dynamic viscoelasticity of SPNs using different 5FBVI-CB[8]-RBVI crosslinkers. Plotting ln λ against ln k_d showed a linear relationship (Fig. 3f), ln $\lambda = -b$ ln k_d + ln A, where $-b$ is the slope and ln A is the intercept. A simplified equation is obtained with $\lambda = Ak_d^{-b}$, where $A = 1.1 \times 10^{-3}$ and $b = 2.2$.

Unveiling the connection between λ and k_d is not trivial, and previous reports have suggested a simple relationship[19] ($\lambda = k_d^{-1}$); however, these reports are based on well-defined SPNs that exhibit close to their sol-gel transition point. Quantifying this relationship in a highly viscoelastic, complex SPN has, so far, not been feasible as there are currently no in situ techniques to directly probe k_d. On the basis of the low k_d values of the SPNs reported here, we have been able to show the connection between λ and k_d in a non-ideal transient network.

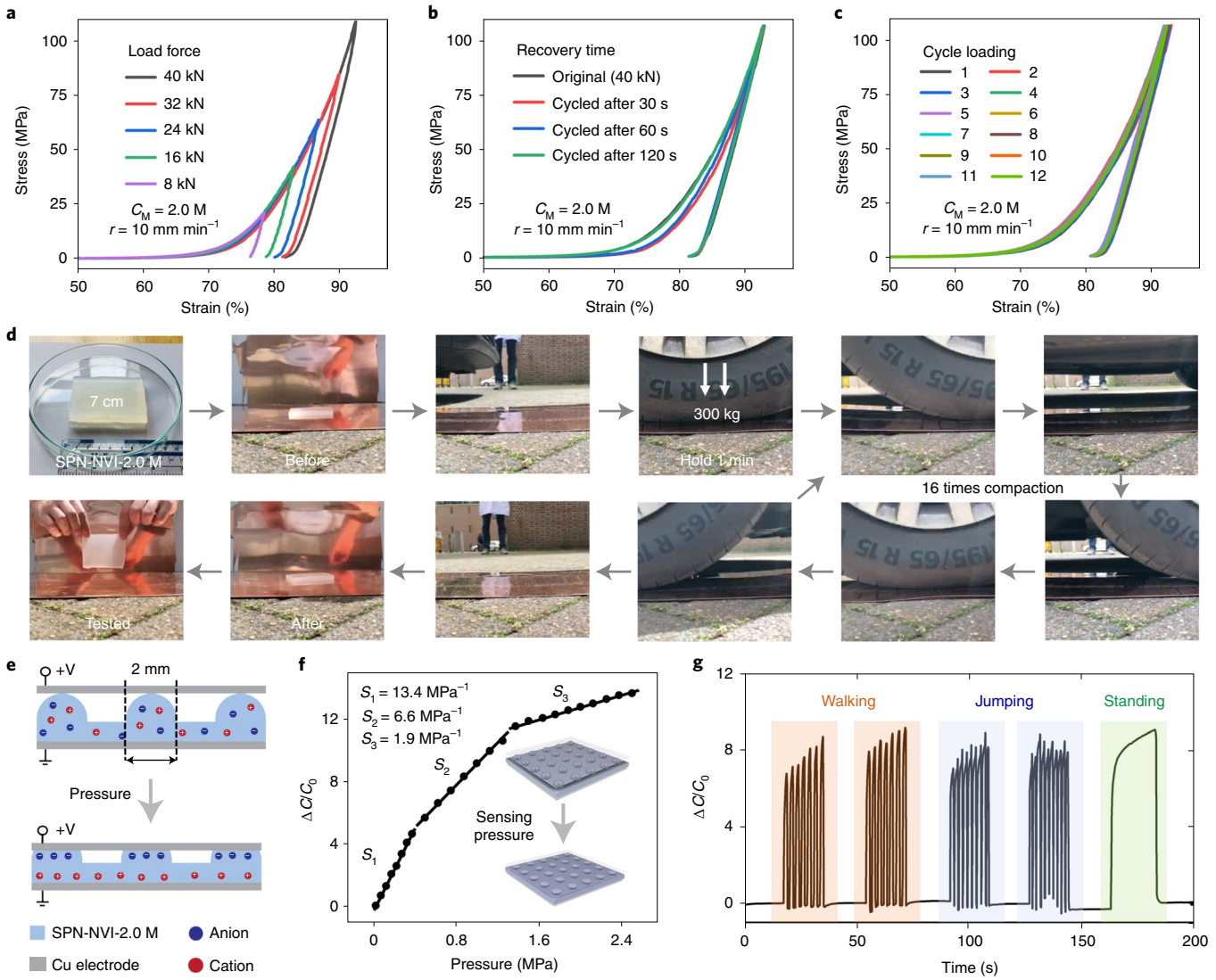

Fig. 5 | Demonstration of rapid self-recovery of glass-like SPNs and their application. a, Compression–retraction stress–strain curves obtained by compressing a specimen at different load forces. **b**, Cyclic compressive stress–strain curves obtained by compressing a specimen at a load force of 40 kN with variable times between consecutive cycles. **c**, Multi-cycle compressive stress–strain curves obtained by compressing a specimen at a load force of 40 kN for 12 cycles with 120 s between each cycle. **d**, Photographs of a car-compression test carried out by compressing a 70 (*L*) × 50 (*W*) × 6 (*T*) mm cuboid specimen with a 1,200 kg four-wheel car for 1 min followed by 16 consecutive effects. **e**, Schematic representation for a SPN-based capacitive pressure sensor using a 20 (*L*) × 20 (*W*) × 2 (*T*) mm specimen with a 5 × 5 matrix of 2 mm (*D*) × 2 mm (*H*) dome-shaped surface structures. **f**, Plot of relative capacitance and pressure to show sensitivity, $S = \mathrm{d}(\Delta C/C_0)/\mathrm{d}P$. **g**, Real-time monitoring plot of relative capacitance for three different motions including walking, jumping and standing (80 kg human).

Compressive properties of glass-like SPNs

Having access to glass-like SPNs with slow crosslink dissociation kinetics leads us to investigate their compressibility and probes self-recovery within these materials. A typical compressive test was carried out on a preformed cylindrical SPN by uniaxially compressing the specimen until the load force or strain was reached (Fig. 4a). Five SPNs, crosslinked by 2.5 mol% 5FBVI-CB[8]-RBVI (RBVI is equal to NVI, diMeBVI, ClBVI, BVI and CNBVI) at $C_M = 2.0$ M, were tested until maximum strain (93%) of the universal test machine and the corresponding stress–strain curves (Fig. 4b).

The SPN with the slowest dissociative crosslink, 5FBVI-CB[8]-NVI (blue set), exhibited the highest compressive strength of 100 MPa. The compressive strength was found to increase across the series in correlation with a decrease of k_d, which could be tuned between 10–100 MPa. Notably, none of the SPN samples fractured at the maximum strain, even the 5FBVI-CB[8]-NVI-crosslinked SPN, which showed the highest strength. To further explore the ultimate strength of these glass-like materials, a series of SPNs crosslinked by 2.5 mol% 5FBVI-CB[8]-NVI were prepared through varying the total monomer concentration ($C_M = 1.0$–6.0 M, solid content was 11–56 wt%, Fig. 4c).

A maximum compressive strength was found up to 1.04 GPa for the 5FBVI-CB[8]-NVI-crosslinked SPN at $C_M = 6.0$ M without any observed fracture at 93% strain. To contextualize our findings, we compared them to other analogous materials known to display high compressive strengths. In Fig. 4d and Supplementary Table 3, the compressive strengths of a range of single- and double-network gels (black) are shown as well as those reported for bovine articular cartilage (blue). The values found for the SPN materials reported here (red) surpass both gels and the bovine cartilage by at least one order

of magnitude. Additionally, despite a composition of up to 80% water, the compressive performance of our glass-like SPNs exceeds bulk materials such as elastomers[44–47]. These results highlight the extreme compressibility and ultra-high strength of glass-like SPNs formed from 5FBVI-CB[8]-RBVI crosslinkers, representing an important milestone in high-performance soft materials.

Cyclic compressive tests were carried out to study the self-recovery of SPNs with 2.5 mol% 5FBVI-CB[8]-NVI crosslinkers at $C_M = 2.0$ M. Compression–retraction cycles at different load forces from 8 to 40 kN are shown in Fig. 5a, demonstrating quasi-plastic deformation, for which the dynamic host–guest interactions play a critical role. This confirms the effective energy dissipation attributed to force-induced rupture of host–guest crosslinkers as sacrificial bonds, similar to other reported supramolecular networks[31,48], Furthermore, a fast and complete self-recovery after 120 s between consecutive cycles was observed (Fig. 5b). This is on account of the slow-dissociative crosslinks within the SPN that can act as quasi-chemical crosslinks to form an elastic network, leading to rapid recovery through elastic retraction and re-association of host–guest complexes.

Multi-cycle compressive tests at the highest force load (40 kN) were performed to study the cyclic compressibility of the glass-like SPNs. Stress–strain curves obtained, for example SPN (2.5 mol% 5FBVI-CB[8]-NVI crosslinkers at $C_M = 2.0$ M, Fig. 5c), showed almost perfect overlap across 12 cycles, demonstrating highly reversible compressibility of the SPN at ultra-high strength of 100 MPa. To further emphasize the extreme compressibility of our SPNs, a large specimen with 70 (L) × 50 (W) × 6 (T) mm (where L is length, W is width and T is thickness) was prepared for a car-compression test (Fig. 5d). A four-wheel car with a total weight of 1,200 kg was driven and held on top of the specimen for 1 min placed between two copper sheets to avoid any slippage or surface contamination. Subsequently, the car repeatedly compacted the specimen 16 times as shown in Supplementary Video 4, and no fracture or irreversible deformation was observed on account of complete self-recovery.

To demonstrate the use of our materials for bioelectronic applications, we fabricated a hydrogel-based capacitive pressure sensor. The dome-shaped structures were included on the surface of the SPN to improve the sensitivity (Fig. 5e). Compared to previous reports (Supplementary Table 4), our hydrogel-based sensor enables access to ultra-high working pressures up to 2.5 MPa, while exhibiting considerable sensitivity (Fig. 5f). Incorporating this sensor under the sole of a human foot, real-time monitoring of three motions (walking, jumping, standing) was successfully achieved (Fig. 5g). These results highlight the ultra-compressibility of our glass-like SPNs and display their potential applicability in prosthetics legs and/or arms and soft robotic skin[49,50].

Outlook

In conclusion, we have successfully introduced a general strategy to incorporate slow-dissociative, non-covalent crosslinkers for the fabrication of glass-like SPNs. On account of these kinetically stable crosslinks, the resultant networks are extremely compressible exhibiting an ultra-high strength up to 1.0 GPa and no fracture observed at 93% strain. The materials also demonstrate rapid room-temperature self-recovery over multiple cycles resulting from the slow-dissociative supramolecular interactions that can act as both sacrificial bonds and quasi-permanent crosslinks. Our approach highlights how to harness control over the crosslink dynamics within SPNs through rational molecular design, which leads to unprecedented, tuneable bulk material properties. A universal scaling law ($\lambda = Ak_d^{-b}$) that applies for both rubber-like and glass-like networks is reported, which completes the overall picture of dynamic mechanics for SPNs. This work provides a general platform to exploit slow-dissociative crosslinks in the design and construction of highly compressible soft materials, holding great promise for myriad applications including artificial muscles, tissue engineering, soft robotics and wearable bioelectronics.

Online content

Any methods, additional references, Nature Research reporting summaries, source data, extended data, supplementary information, acknowledgements, peer review information; details of author contributions and competing interests; and statements of data and code availability are available at https://doi.org/10.1038/s41563-021-01124-x.

Received: 18 December 2020; Accepted: 7 September 2021;
Published online: 25 November 2021

References

1. Seiffert, S. & Sprakel, J. Physical chemistry of supramolecular polymer networks. *Chem. Soc. Rev.* **41**, 909–930 (2012).
2. Voorhaar, L. & Hoogenboom, R. Supramolecular polymer networks: hydrogels and bulk materials. *Chem. Soc. Rev.* **45**, 4013–4031 (2016).
3. Sun, T. L. et al. Physical hydrogels composed of polyampholytes demonstrate high toughness and viscoelasticity. *Nat. Mater.* **12**, 932–937 (2013).
4. Wu, Y. et al. Biomimetic supramolecular fibers exhibit water-induced supercontraction. *Adv. Mater.* **30**, 1707169 (2018).
5. Jeon, I., Cui, J., Illeperuma, W. R. K., Aizenberg, J. & Vlassak, J. J. Extremely stretchable and fast self-healing hydrogels. *Adv. Mater.* **28**, 4678–4683 (2016).
6. Li, C.-H. et al. A highly stretchable autonomous self-healing elastomer. *Nat. Chem.* **8**, 618–624 (2016).
7. Sun, G., Li, Z., Liang, R., Weng, L.-T. & Zhang, L. Super stretchable hydrogel achieved by non-aggregated spherulites with diameters <5 nm. *Nat. Commun.* **7**, 12095 (2016).
8. Cordier, P., Tournilhac, F., Soulié-Ziakovic, C. & Leibler, L. Self-healing and thermoreversible rubber from supramolecular assembly. *Nature* **451**, 977–980 (2008).
9. Chen, Y., Kushner, A. M., Williams, G. A. & Guan, Z. Multiphase design of autonomic self-healing thermoplastic elastomers. *Nat. Chem.* **4**, 467–472 (2012).
10. Yanagisawa, Y., Nan, Y., Okuro, K. & Aida, T. Mechanically robust, readily repairable polymers via tailored noncovalent cross-linking. *Science* **359**, 72–76 (2018).
11. Qin, B. et al. Tough and multi-recyclable cross-linked supramolecular polyureas via incorporating noncovalent bonds into main-chains. *Adv. Mater.* **32**, 2000096 (2020).
12. Wang, C. et al. Self-healing chemistry enables the stable operation of silicon microparticle anodes for high-energy lithium-ion batteries. *Nat. Chem.* **5**, 1042–1048 (2013).
13. Choi, S., Kwon, T.-w, Coskun, A. & Choi, J. W. Highly elastic binders integrating polyrotaxanes for silicon microparticle anodes in lithium ion batteries. *Science* **357**, 279–283 (2017).
14. Tee, B. C.-K., Wang, C., Allen, R. & Bao, Z. An electrically and mechanically self-healing composite with pressure- and flexion-sensitive properties for electronic skin applications. *Nat. Nanotechnol.* **7**, 825–832 (2012).
15. Liu, K., Jiang, Y., Bao, Z. & Yan, X. Skin-inspired electronics enabled by supramolecular polymeric materials. *CCS Chem.* **1**, 431–447 (2019).
16. Dankers, P. Y. W. et al. Hierarchical formation of supramolecular transient networks in water: a modular injectable delivery system. *Adv. Mater.* **24**, 2703–2709 (2012).
17. Zhang, S. et al. A ph-responsive supramolecular polymer gel as an enteric elastomer for use in gastric devices. *Nat. Mater.* **14**, 1065–1071 (2015).
18. Yount, W. C., Loveless, D. M. & Craig, S. L. Strong means slow: dynamic contributions to the bulk mechanical properties of supramolecular networks. *Angew. Chem. Int. Ed.* **44**, 2746–2748 (2005).
19. Yount, W. C., Loveless, D. M. & Craig, S. L. Small-molecule dynamics and mechanisms underlying the macroscopic mechanical properties of coordinatively cross-linked polymer networks. *J. Am. Chem. Soc.* **127**, 14488–14496 (2005).
20. Grindy, S. C. et al. Control of hierarchical polymer mechanics with bioinspired metal-coordination dynamics. *Nat. Mater.* **14**, 1210–1216 (2015).
21. Appel, E. A., del Barrio, J., Loh, X. J. & Scherman, O. A. Supramolecular polymeric hydrogels. *Chem. Soc. Rev.* **41**, 6195–6214 (2012).
22. Xia, D. et al. Functional supramolecular polymeric networks: the marriage of covalent polymers and macrocycle-based host-guest interactions. *Chem. Rev.* **120**, 6070–6123 (2020).
23. Wang, L. et al. A self-cross-linking supramolecular polymer network enabled by crown-ether-based molecular recognition. *J. Am. Chem. Soc.* **142**, 2051–2058 (2020).
24. Shi, C.-Y. et al. An ultrastrong and highly stretchable polyurethane elastomer enabled by a zipper-like ring-sliding effect. *Adv. Mater.* **32**, 2000345 (2020).

25. Harada, A., Kobayashi, R., Takashima, Y., Hashidzume, A. & Yamaguchi, H. Macroscopic self-assembly through molecular recognition. *Nat. Chem.* **3**, 34–37 (2011).
26. Gotoh, H. et al. Optically transparent, high-toughness elastomer using a polyrotaxane cross-linker as a molecular pulley. *Sci. Adv.* **4**, eaat7629 (2018).
27. Ogoshi, T., Kayama, H., Yamafuji, D., Aoki, T. & Yamagishi, T.-a Supramolecular polymers with alternating pillar[5]arene and pillar[6]arene units from a highly selective multiple host–guest complexation system and monofunctionalized pillar[6]arene. *Chem. Sci.* **3**, 3221–3226 (2012).
28. Li, Z.-Y. et al. Cross-linked supramolecular polymer gels constructed from discrete multi-pillar[5]arene metallacycles and their multiple stimuli-responsive behavior. *J. Am. Chem. Soc.* **136**, 8577–8589 (2014).
29. Wang, X.-H. et al. Efficient aggregation-induced emission manipulated by polymer host materials. *Adv. Mater.* **31**, 1903962 (2019).
30. Xu, W., Song, Q., Xu, J.-F., Serpe, M. J. & Zhang, X. Supramolecular hydrogels fabricated from supramonomers: a novel wound dressing material. *ACS Appl. Mater. Interfaces* **9**, 11368–11372 (2017).
31. Liu, J. et al. Tough supramolecular polymer networks with extreme stretchability and fast room-temperature self-healing. *Adv. Mater.* **29**, 1605325 (2017).
32. Lee, J. W., Samal, S., Selvapalam, N., Kim, H.-J. & Kim, K. Cucurbituril homologues and derivatives:new opportunities in supramolecular chemistry. *Acc. Chem. Res.* **36**, 621–630 (2003).
33. Lagona, J., Mukhopadhyay, P., Chakrabarti, S. & Isaacs, L. The cucurbit[n]uril family. *Angew. Chem. Int. Ed.* **44**, 4844–4870 (2005).
34. Urbach, A. R. & Ramalingam, V. Molecular recognition of amino acids, peptides, and proteins by cucurbit[n]uril receptors. *Isr. J. Chem.* **51**, 664–678 (2011).
35. Ni, X.-L. et al. Cucurbit[n]uril-based coordination chemistry: from simple coordination complexes to novel poly-dimensional coordination polymers. *Chem. Soc. Rev.* **42**, 9480–9508 (2013).
36. Assaf, K. I. & Nau, W. M. Cucurbiturils: from synthesis to high-affinity binding and catalysis. *Chem. Soc. Rev.* **44**, 394–418 (2015).
37. Barrow, S. J., Kasera, S., Rowland, M. J., del Barrio, J. & Scherman, O. A. Cucurbituril-based molecular recognition. *Chem. Rev.* **115**, 12320–12406 (2015).
38. Huang, Z. et al. Host-enhanced phenyl-perfluorophenyl polar-π interactions. *J. Am. Chem. Soc.* **142**, 7356–7361 (2020).
39. Biedermann, F., Vendruscolo, M., Scherman, O. A., De Simone, A. & Nau, W. M. Cucurbit [8] uril and blue-box: high-energy water release overwhelms electrostatic interactions. *J. Am. Chem. Soc.* **135**, 14879–14888 (2013).
40. Bell, R. P. & Hinshelwood, C. N. The theory of reactions involving proton transfers. *Proc. Math. Phys. Eng. Sci.* **154**, 414–429 (1936).
41. Evans, M. G. & Polanyi, M. Further considerations on the thermodynamics of chemical equilibria and reaction rates. *Trans. Faraday Soc.* **32**, 1333–1360 (1936).
42. Burnouf, D. et al. kinitc: a new method for obtaining joint thermodynamic and kinetic data by isothermal titration calorimetry. *J. Am. Chem. Soc.* **134**, 559–565 (2012).
43. Huang, Z. et al. Supramolecular chemistry of cucurbiturils: tuning cooperativity with multiple noncovalent interactions from positive to negative. *Langmuir* **32**, 12352–12360 (2016).
44. Sheppard, J. & Clapson, W. Compression stress strain of rubber. *Rubber Chem. Technol.* **6**, 126–150 (1933).
45. Elleuch, R., Elleuch, K., Salah, B. & Zahouani, H. Tribological behavior of thermoplastic polyurethane elastomers. *Mater. Des.* **28**, 824–830 (2007).
46. Gerratt, A. P., Michaud, H. O. & Lacour, S. P. Elastomeric electronic skin for prosthetic tactile sensation. *Adv. Func. Mater.* **25**, 2287–2295 (2015).
47. Lee, W., Yeo, K., Andriyana, A., Shee, Y. & Adikan, F. M. Effect of cyclic compression and curing agent concentration on the stabilization of mechanical properties of pdms elastomer. *Mater. Des.* **96**, 470–475 (2016).
48. Park, J. et al. Extremely rapid self-healable and recyclable supramolecular materials through planetary ball milling and host–guest interactions. *Adv. Mater.* **32**, 2002008 (2020).
49. Hammock, M. L., Chortos, A., Tee, B. C.-K., Tok, J. B.-H. & Bao, Z. 25th anniversary article: the evolution of electronic skin (e-skin): a brief history, design considerations, and recent progress. *Adv. Mater.* **25**, 5997–6038 (2013).
50. Chortos, A., Liu, J. & Bao, Z. Pursuing prosthetic electronic skin. *Nat. Mater.* **15**, 937–950 (2016).

Methods

Materials. Unless otherwise stated, all the chemicals used in the present work were purchased from Sigma Aldrich and directly used without further purification: acrylamide (for molecular biology, 99%, high-performance liquid chromatography (HPLC)), 1-vinylimidazole (99%), 2,3,4,5,6-perfluorobenzyl bromide (99%), benzyl bromide (reagent grade, 98%), 2-(bromomethyl)naphthalene (96%), 2,3-dimethylbenzyl bromide (Aldrich Partner Apollo Scientific Ltd, 95%), 4-methoxylbenzyl bromide (95%), 4-methylbenzyl bromide (96%), 4-iodobenzyl bromide (95%), 4-bromobenzyl bromide (98%), 4-chlorobenzyl bromide (97%), 4-fluorobenzyl bromide (97%), 4-(bromomethyl)benzonitrile (99%), 4-nitrobenzyl bromide (99%), 2-naphthyl isocyanate (97%), *N*-hydroxyethyl acrylamide (97%, 1,000 ppm MEHQ), acetonitrile (HPLC, 99.9%), ethanol (absolute, 99.8%, HPLC), acetone (ACS reagent, 99.5%), diethyl ether (ACS reagent, 99%), deuterium oxide (D_2O, D 99.8 at.%), dimethyl sufoxide-d_6 (DMSO-d_6, D 99.9 at.%), nitrogen, 2-hydroxy-4′-(2-hydroxyethoxy)-2-methylpropiophenone (photoinitiator, I-2959, 98%) and 1,2-bis(2-(4,5-dihydro-1*H*-imidazol-2-yl)propan-2-yl)diazene dihydrochloride (Aldrich Partner, Ambeed, Inc., thermoinitiator, VA-044, 95%). Cucurbit[8]uril was synthesized and isolated in 100-g scale from the mixture of cucurbit[n]uril derivatives using a conventional protocol. Milli-Q water was obtained from a Milli-Q Integral Water Purification System (18.2 MΩ cm^{-1}). Unless otherwise noted, all the sample solutions for characterization were prepared in D_2O or Milli-Q H_2O under heating and ultrasonication.

Monomer synthesis. All the guest monomers were readily synthesized through salt formation reaction between different substituted benzyl bromide (10.0 mmol) and 1-vinylimidazole (15.0 mmol) through stirring in acetonitrile (20 ml) at 82 °C for 12 h. After reaction, the mixture was divided into two portions in two Falcon tubes. Then, 30 ml of diethyl ether was added into each of the tubes to precipitate the imidazolium salt from the reaction mixture. The white solid of imidazolium salt was was collected by centrifugation at 10,000 r.p.m. for 10 min at 4 °C to remove the supernatant containing excess 1-vinylimidazole. After that, the crude product was washed by 40 ml diethyl ether in each tube and centrifuged again. Eventually, the white imidazolium product was combined and dried in a vacuum oven at 50 °C until a constant weight was reached.

SPN fabrication. Certain amounts of acrylamide, non-covalent crosslinker (5FBVI-RBVI-CB[8]) and photoinitiator (I-2959) were predetermined (Supplementary Table 5), weighed out in a glass vial and dissolved (or dispersed) in Milli-Q water with the precalculated volume under ultrasonication for 10 min. The resultant precursor solution (or suspension) was sealed and purged with nitrogen for at least 30 min to remove residual oxygen in the solution phase, which may eliminate radicals during polymerization. The precursor solution was carefully injected into a laboratory-made glass mould until the whole mould was filled without any bubble or spare space. The glass mould filled with the precursor solution was exposed to ultraviolet irradiation at 350 nm with 4.8 mW cm^{-2} for 6 h to undergo in situ photopolymerization. After one-pot polymerization, the SPNs was removed from the glass mould and further cut into the test specimens with certain sizes and shapes using a dumbbell/cylinder-shaped cutter or a razor blade. The prepared SPNs were directly used in the subsequent characterization or demonstration without further purification. As the relatively long polymerization time is used, the residual amount of acrylamide is less than 1%, which will not be problematic for further application.

ITC. ITC experiments were conducted on a Malvern MicroCal Auto-ITC200 apparatus at 298.15 K in Milli-Q H_2O. In a typical titration to study secondary binding, the solution of 1:1 complex (5FBVI-CB[8]) was loaded in the sample cell at a concentration of 0.5 mM, and the second guest molecule was loaded in the syringe at a tenfold higher concentration of 5.0 mM. One titration experiment consisted of one injection of 0.6 µl and 32 consecutive injections of 1.2 µl with 90 s intervals between injections. The first one or two data points were removed before data analysis as they may contain contamination, and the resultant ITC curves were fitted by one set of sites model within Malvern MicroCal Analysis Centre software to gain thermodynamic information on the secondary binding (K_{eq}, ΔH, ΔS). The ITC data were further analysed using a kinITC method, using Affinimeter-ITC-Advanced software, to obtain association/dissociation kinetic rate constants for the secondary binding (k_a, k_d). All the titrations were repeated for three times to provide the average values with their corresponding error bars.

Rheology. Rheological characterization was implemented by a Discovery Hybrid Rheometer (DHR)-2, TA Instruments, with a Peltier Plate for temperature control. All the measurements were conducted on a 20-mm parallel stain steel plate geometry with a fixed gap at 1,500 µm, and the necessary calibration for geometry was carried out before testing. All the samples for rheological characterization were measured just after the SPN fabrication. Oscillatory frequency-sweep measurements were conducted at 1.0% strain in the frequency range from 0.1 to 100 rad s^{-1}. Continuous step-strain measurements were performed at 1.0 rad s^{-1} in high-amplitude oscillatory (500% strain) and low-amplitude oscillatory (5.0% strain), respectively. The above data were collected at 293.15 K and analysed using TRIOS software, TA Instruments. TTS experiments were conducted on a series of frequency-sweep measurements from 0.016 to 16.0 Hz at 1% strain in the temperature range from 273.15 to 353.15 K with 10 K intervals. For each temperature, the frequency-sweep curve was shifted horizontally with a temperature-dependent shift factor α_T, using 303.15 K (30 °C) as the reference temperature ($\alpha_{30} = 1$). Time–kinetics superposition experiments were carried out on a series of frequency-sweep measurements from 0.016 to 16.0 Hz at 1% strain and 298.15 K (to be consistent with kinITC dataset) using 11 different SPNs with distinct non-covalent crosslinkers. For each SPN, the frequency-sweep curve was shifted horizontally with a kinetics-dependent shift factor λ_{RBVI}, using BVI as the reference guest ($\lambda_{BVI} = 1$). Through plot and linear fit for ln λ and ln k_d, the quantitative relationship between dynamic mechanical property and crosslink dissociation kinetics was revealed.

Compression. Compressive tests were conducted, just after the SPN fabrication, on a Tinius Olsen Model 50ST Benchtop Tester equipped with a 50-kN load cell at room temperature. In a typical compressive test, a cylinder specimen with a fixed shape (22 mm D × 7 mm H, where D is diameter and H is height) was placed between two stain steel plates and compressed at a specific deformation rate (10 mm min^{-1}) to obtain the stress–strain curve. Cyclic compressive tests with variable waiting time (0–120 s) were further carried out to study self-recovery of the resultant glass-like SPNs. Compressing-retraction cycles were obtained by compressing cylinder specimens until set load forces from 8 to 40 kN with 8-kN intervals. Multi-cycle compressive tests were performed by compressing a cylinder specimen until the highest load force (40 kN) at a rate of 10 mm min^{-1}, relaxing the specimen at the same deformation rate and repeating the above two steps as one whole cycle for 12 times with 2 min waiting time between cycles.

Capacitive pressure sensor. To improve sensitivity of pressure sensor in the high-pressure range above 100 kPa, a SPN specimen (20 mm L × 20 mm W × 2 mm T) with a 5 × 5 matrix of dome structures (2 mm D × 2 mm H) was designed and used. This specimen was prepared similarly to the above SPNs, using a flat, transparent glass mould along with a polylactic acid mould containing defined holes complementary to dome-shaped structures (fabricated by an Ultimaker 2, three-dimensional printer). The prepared pressure sensor with dome structures was tested with a universal test machine (Tinius Olsen Model 50ST Benchtop Tester) and a LCR meter (Compact LCR Meter ST2830). By compressing the sensor with the universal test machine (1–1,000 N) and recording the capacitance simultaneously, a plot of capacitance and stress was obtained. Through linear fit, the average sensitivity was calculated in their corresponding pressure range (S_1, S_2, S_3). The use of the obtained pressure sensor was further demonstrated by sensing human motions on a foot. Through monitoring the capacitance, a real-time plot of capacitance variation was obtained to show three different human motions including 2 × 10 s of walking, 2 × 10 s of jumping and 10 s of standing with a 10 s pause between each motion.

Data availability

Data generated and analysed during this study are provided as source data with this paper or included in the Supplementary Information. Further data are available from the corresponding authors upon request.

Acknowledgements

O.A.S. and G.W. acknowledge the Leverhulme Trust Program Grant (Natural Materials Innovation). Z.H. acknowledges the Marie Skłodowska-Curie Fellowship (no. 845640). X.C. acknowledges Cambridge Display Technology (CDT) for financial support. D.J.W. thanks the Engineering and Physical Sciences Research Council for a PhD studentship (grant no. EP/R512461/1). We thank G.G. Malliaras for helpful discussions.

Author contributions

Z.H. and O.A.S. conceived the idea. Z.H., X.C., S.J.K.O., G.W., D.J.W., J.A.M. and O.A.S. designed the experiments. Z.H. executed most of the experiments and analysed the data. X.C., S.J.K.O., G.W., D.J.W., J.L. and J.A.M. helped perform some of the experiments and data analysis. Z.H., J.A.M. and O.A.S. wrote the paper. All authors discussed the experiments, edited the paper and gave consent for this publication under the supervision of O.A.S.

Competing interests

The authors declare no competing interests.

Additional information

Supplementary information The online version contains supplementary material available at https://doi.org/10.1038/s41563-021-01124-x.

Correspondence and requests for materials should be addressed to Oren A. Scherman.

Peer review information *Nature Materials* thanks Richard Hoogenboom, Rebecca Kramer-Bottiglio and Mathew Webber for their contribution to the peer review of this work.

Reprints and permissions information is available at www.nature.com/reprints.